J Solid State Electrochem (2003) 7: 645–650
DOI 10.1007/s10008-003-0423-7

ORIGINAL PAPER

T. A. Zotov · V. N. Verbetsky · T. Y. Safonova
O. A. Petrii

Nonstoichiometric Ti-Zr-Ni-V-Mn alloys: the effect of composition on hydrogen sorption and electrochemical characteristics

Received: 18 April 2003 / Accepted: 25 June 2003 / Published online: 29 August 2003

Abstract The effect of the stoichiometric factor on the electrochemical and gas-phase behavior of hydride-forming intermetallic alloys of the $Ti_{0.45}Zr_{0.55}Ni_y$-$V_{0.45}Mn_x$ general composition is studied. The structure and the phase composition of the alloys were investigated by means of X-ray diffraction, electron microscopy, and electron probe microanalysis. An introduction of hydrogen does not change the structure type and hydriding is accompanied by an isotropic increase in the cell volume by about 20%. The alloys studied demonstrate maximum values of hydrogen sorption capacity, discharge capacity, and good rate capability throughout a wide range of compositions, rather than in a narrow region in the vicinity of the stoichiometric composition.

Keywords MH electrodes · Intermetallic compounds (IMC) · Crystal structure · Hydrogen absorption · Discharge capacity

Introduction

Being one of the central problems of modern electrochemistry, the problem of synthesizing and characterizing electrode materials for chemical power sources did not escaped the attention of Professor W. Vielstich [1, 2]. This paper deals with materials for nickel-metal hydride (Ni-MH) batteries. These batteries are widely adopted today for their high energy characteristics and good environmental compatibility [3, 4]. For our studies, we have chosen the Laves phase type intermetallic compounds (IMC) of the Ti-Zr-Ni-V-Mn system. The basis of these IMCs is the Ti-Zr-Mn system with a wide homogeneity region of the Laves phase (the homogeneity regions of binary systems involved are about $TiMn_{1.3(1.25)}$-$TiMn_{1.9(2.0)}$ and $ZrMn_{1.9(1.8)}$-$ZrMn_{2.9(3.4)}$ [5, 6, 7, 8, 9]). Addition of vanadium provides an increase in the hydrogen absorption. The addition of nickel is necessary to enhance the catalytic activity of alloys. The Ti-Zr-Ni-V-Mn system was studied quite extensively [3, 4, 10, 11, 12, 13, 14, 15, 16, 17] largely as a part of the active search for compositions with significant discharge characteristics. In this work, taking into account the results of previous studies, we have chosen these compositions suitable for studying the role the alloy nonstoichiometry plays in defining the hydrogen sorption properties.

Three series of alloys with various nickel and manganese contents ($Ti_{0.45}Zr_{0.55}Ni_{1.0}V_{0.45}Mn_x$, $x = 0.09$–0.28; $Ti_{0.45}Zr_{0.55}Ni_{0.85}V_{0.45}Mn_x$, $x = 0.1$–1.33; and $Ti_{0.45}Zr_{0.55}Ni_{0.70}V_{0.45}Mn_x$, $x = 0.08$–1.47) were prepared. The preliminary results were published in [18] and reported at the International Symposium on Metal Hydrogen Systems 2002 [19].

Experimental

Alloys were prepared by arc-melting the mixtures of initial metals under argon atmosphere. With the purpose of homogenization, the alloy samples were annealed for 240 h at 850 °C with subsequent quenching in cold water. The phase composition of alloys was examined on polished cross sections of the ingots by a scanning electron microscope (SEM) with energy dispersive X-ray analyzer (EDXA JXA-733 with LINK-2 microcomputer system). The crystal structure and lattice parameters were determined by means of powder X-ray diffraction (URD-6 diffractometer with CuK_α). Conditions were: scan range 25–85 with a step size of 0.02° and a sampling time of 1 or 3 s per step. The refinement of diffraction profiles was performed using the Rietveld method.

The ability of alloys to absorb hydrogen from the gas phase was studied by using a Siewert's type apparatus at a pressure below 50 atm. The MH electrodes were prepared by mixing alloy powder with copper powder at a weight ratio IMC:Cu = 1:4. The mixture was cold-pressed to a pellet. The electrochemical experiments were carried out in a three-electrode electrochemical glass cell with separate anodic and cathodic compartments. An MH electrode

Dedicated to Prof. Wolf Vielstich on the occasion of his 80th birthday in recognition of his numerous contributions to interfacial electrochemistry

T. A. Zotov · V. N. Verbetsky · T. Y. Safonova · O. A. Petrii (✉)
Department of Chemistry, Moscow State University,
Leninskie Gory, 3, 119992 Moscow, Russia
E-mail: petrii@elchem.msu.ru

served as the working electrode, platinum served as the counter electrode. As the reference electrode, we used either a reversible hydrogen electrode in the same solution or a Hg/HgO electrode. 6 mol/l KOH (special purity grade) was used as the electrolyte. The preliminary activation of MH electrodes involved boiling in 6 mol/l KOH at about 115 °C for 1.5 h before the first polarization. It was found that after preliminary activation the discharge capacity of MH electrodes studied reaches its maximum in 2–4 cycles. Samples were charged at a current density of 100 mA/g for 6 h. The discharge cut-off potential was +250 mV against the hydrogen reference electrode and −650 mV against the Hg/HgO electrode. The electrodes were discharged at current densities of 100, 200, and 400 mA/g, which allowed us to assess their rate capabilities.

Results and discussion

The results obtained by using electron microscopy, electron probe microanalysis, and powder X-ray diffraction analysis indicate that the main phase present is the Laves phase C14 of the $MgZn_2$ type. A small amount of the MnV phase with a primitive cubic lattice of the CsCl type was present in $Ti_{0.45}Zr_{0.55}Ni_{0.85}V_{0.45}Mn_x$ alloys with $x = 0.77$, 0.94, 1.16, and 1.33 and in $Ti_{0.45}Zr_{0.55}Ni_{0.70}V_{0.45}Mn_x$ with $x = 0.90$, 1.15, 1.33, and 1.47. Moreover, traces (1–2%) of nonstoichiometric zirconium oxide with cubic lattice of the NaCl type are present in all alloys. That is why, the zirconium oxide content is not shown in Table 1. Table 1 shows the phase composition of the alloys and the lattice parameters of the phases present. The table also lists the R-factors of Rietveld calculations. The values of Rwp > 5 correspond to conditions of the X-ray experiments with the exposition time 1 s.

Inasmuch as we deal with non-stoichiometric alloys, we are interested in the effect of stoichiometry factor on their structure. It is known [10] that a part of Ti atoms that occupy the positions of A-atoms in the AB_2-Laves structure can also occupy the positions of B-atoms in sub-stoichiometric IMC. In super-stoichiometric IMC, a part of Mn atoms can pass from B positions to A positions [10].

The occupation of metallic sites in the C14 structure was refined by using the Rietveld method. The minimization of R-factors showed that the best fit is achieved for the following model. For the sub-stoichiometric region (Ti, Zr)(Ti, Ni, V, Mn)$_2$ with a low manganese content, it was found that vanadium atoms totally occupy the 2(a) sites of the C14 structure and titanium, nickel, manganese, and the rest of vanadium atoms occupy the 6(h) sites. The site occupation distribution is somewhat different in the case of super-stoichiometric

Table 1 Structural characteristics of IMC

Alloys composition $Ti_{0.45}Zr_{0.55}Ni_yV_{0.45}Mn_x$	n in AB_n	Phases	a, Å	c, Å	V, Å^{3a}	S^b	R_F^{c}	R_{WP}^{d}
y = 1.0, x = 0.09	$AB_{1.54}$	C14	4.977	8.119	174.15	1.0444	4.08	8.47
y = 1.0, x = 0.19	$AB_{1.64}$	C14	4.965	8.093	172.76	1.0578	3.45	7.55
y = 1.0, x = 0.28	$AB_{1.73}$	C14	4.955	8.077	171.71	1.1485	1.52	5.40
y = 0.85, x = 0.10	$AB_{1.40}$	C14	4.991	8.141	175.81	0.7438	0.77	4.52
y = 0.85, x = 0.18	$AB_{1.48}$	C14	4.972	8.108	173.58	0.7642	1.04	4.59
y = 0.85, x = 0.23	$AB_{1.53}$	C14	4.965	8.096	172.85	0.6866	0.76	3.69
y = 0.85, x = 0.33	$AB_{1.63}$	C14	4.958	8.084	172.06	1.1113	1.76	6.16
y = 0.85, x = 0.53	$AB_{1.83}$	C14	4.947	8.064	170.91	0.6903	0.75	3.58
y = 0.85, x = 0.70	$AB_{2.00}$	C14	4.923	8.021	168.32	0.6729	0.84	3.52
y = 0.85, x = 0.77	$AB_{2.07}$	C14: 96%	4.921	8.016	168.07	0.6436	0.84	3.19
		MnV: 4%	2.938		25.36		0.84	
y = 0.85, x = 0.94	$AB_{2.24}$	C14: 95%	4.915	8.005	167.49	1.0722	2.36	5.26
		MnV: 5%	2.937		25.34		2.50	
y = 0.85, x = 1.16	$AB_{2.46}$	C14: 93%	4.910	7.994	166.93	1.0643	2.42	5.06
		MnV: 7%	2.934		25.26		2.64	
y = 0.85, x = 1.33	$AB_{2.63}$	C14: 91%	4.899	7.974	165.76	0.5987	0.85	2.82
		MnV: 9%	2.926		24.96		0.52	
y = 0.70, x = 0.08	$AB_{1.23}$	C14	5.038	8.213	179.06	1.1238	2.34	10.17
y = 0.70, x = 0.17	$AB_{1.32}$	C14	5.017	8.180	178.26	0.8212	0.91	4.69
y = 0.70, x = 0.35	$AB_{1.50}$	C14	4.986	8.136	175.20	0.6702	0.54	3.57
y = 0.70, x = 0.53	$AB_{1.68}$	C14	4.967	8.105	173.18	0.6979	0.57	3.27
y = 0.70, x = 0.71	$AB_{1.86}$	C14	4.947	8.065	171.02	0.6422	0.55	3.21
y = 0.70, x = 0.90	$AB_{2.05}$	C14: 96%	4.929	8.037	169.10	0.6298	0.83	2.97
		MnV: 4%	2.943		25.49		1.01	
y = 0.70, x = 1.15	$AB_{2.30}$	C14: 95%	4.918	8.010	168.10	0.7752	0.96	4.89
		MnV: 5%	2.935		25.22		1.01	
y = 0.70, x = 1.33	$AB_{2.48}$	C14: 94%	4.906	7.995	167.07	1.0171	2.16	4.49
		MnV: 6%	2.929		25.12		2.59	
y = 0.70, x = 1.47	$AB_{2.62}$	C14: 90%	4.900	7.983	166.65	0.6683	0.54	2.87
		MnV: 10%	2.923		24.96		0.59	

[a] Cell volume

[b] $S = \left\{ \left[\sum w_i (y_i(\exp) - y_i(calc))^{1/2} \right] \Big/ (N - P) \right\}^{1/2}$, (N=number of experimental points, P=number of refined parameters

[c] $R_F = \sum \left| I^{1/2}(\exp) - I^{1/2}(calc) \right| \Big/ \sum I^{1/2}(\exp)$

[d] $R_{wp} = \left\{ \sum w_i [y_i(\exp) - y_i(calc)]^2 \Big/ \sum w_i [y_i(\exp)]^2 \right\}^{1/2}$

region (Ti, Zr, Mn)(Ni, V, Mn)$_2$ with a high Mn content. Here, vanadium and manganese atoms occupy the 2(a) sites; nickel and manganese atoms occupy the 6(h) sites.

The lattice parameters of the C14 Laves phase were found to decrease with an increase in the manganese content in the alloy, as shown in Fig. 1.

The hydrogen sorption from the gas phase was studied for all the $Ti_{0.45}Zr_{0.55}Ni_yV_{0.45}Mn_x$ alloys. The introduction of hydrogen does not change the structure type and the hydriding is accompanied by isotropic

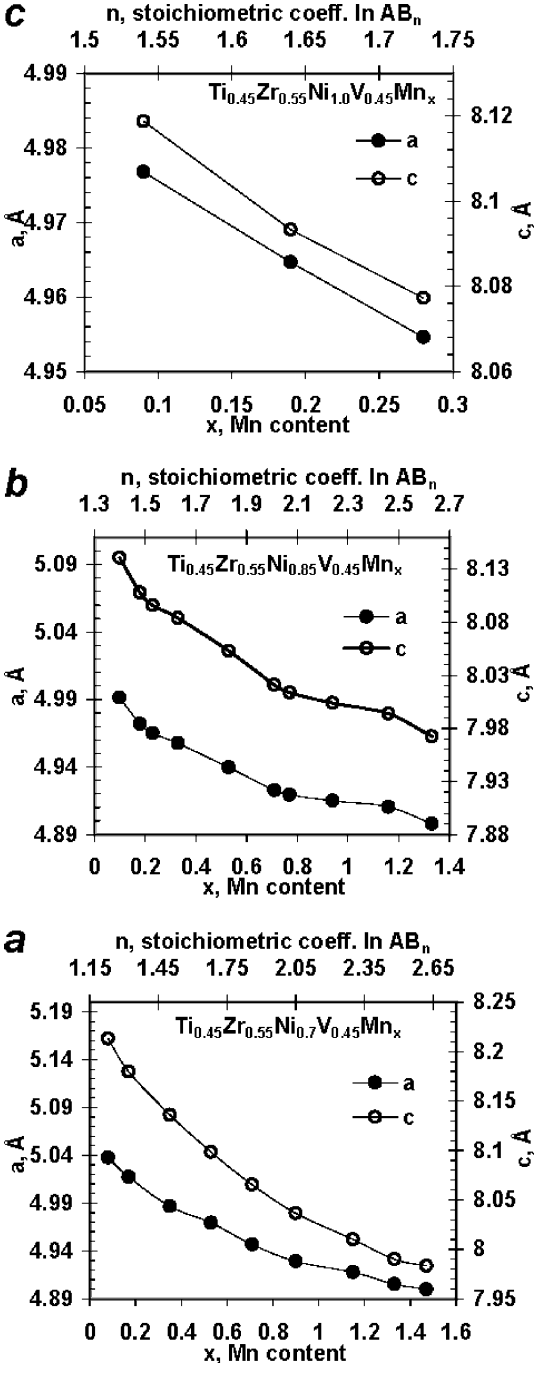

Fig. 1a–c Lattice parameters of: **a** $Ti_{0.45}Zr_{0.55}Ni_{0.70}V_{0.45}Mn_x$; **b** $Ti_{0.45}Zr_{0.55}Ni_{0.85}V_{0.45}Mn_x$; **c** $Ti_{0.45}Zr_{0.55}Ni_{1.0}V_{0.45}Mn_x$

Table 2 Hydrogen absorption and electrochemical properties of $Ti_{0.45}Zr_{0.55}Ni_yV_{0.45}Mn_x$ alloys

Alloys composition $Ti_{0.45}Zr_{0.55}Ni_yV_{0.45}Mn_x$	n in AB_n	$C_{i=100}/C_{i=200}/C_{i=400}$, mAh/g	P eq., atm.	Hydrogen content, mass %	Rate capability $C_{i=400}/C_{i=100}$	Lattice expansion $\Delta V_{hydr}/V_{IMC}$, %
y = 1.0, x = 0.09	$AB_{1.54}$	389/369/336	< 0.01	1.80	0.86	18.4
y = 1.0, x = 0.19	$AB_{1.64}$	323/317/295	0.044	1.80	0.91	19.9
y = 1.0, x = 0.28	$AB_{1.73}$	339/334/320	0.089	1.85	0.94	19.7
y = 0.85, x = 0.10	$AB_{1.40}$	240/167/120	< 0.01	1.93	0.50	–
y = 0.85, x = 0.18	$AB_{1.48}$	318/297/255	< 0.01	1.78	0.80	–
y = 0.85, x = 0.23	$AB_{1.53}$	360/334/288	~0.02	1.98	0.80	18.7
y = 0.85, x = 0.33	$AB_{1.63}$	312/300/279	0.03	1.71	0.90	–
y = 0.85, x = 0.53	$AB_{1.83}$	262/250/217	0.28	1.82	0.83	–
y = 0.85, x = 0.70	$AB_{2.00}$	391/376/324	1.16	2.04	0.88	–
y = 0.85, x = 0.77	$AB_{2.07}$	215/213/212	–	–	0.97	–
y = 0.85, x = 0.94	$AB_{2.24}$	178/178/176	–	–	0.99	–
y = 0.70, x = 0.08	$AB_{1.23}$	21/10/5	< 0.01	1.96	0.24	17.9
y = 0.70, x = 0.17	$AB_{1.32}$	127/80/50	< 0.01	1.62	0.39	20.7
y = 0.70, x = 0.35	$AB_{1.50}$	160/97/53	< 0.02	1.69	0.33	19.0
y = 0.70, x = 0.53	$AB_{1.68}$	178/102/58	< 0.02	1.69	0.33	23.6
y = 0.70, x = 0.71	$AB_{1.86}$	296/250/153	0.23	1.86	0.52	20.9
y = 0.70, x = 0.90	$AB_{2.05}$	315/255/145	1.0	2.01	0.46	–
y = 0.70, x = 1.15	$AB_{2.30}$	258/210/128	–	–	0.50	–
y = 0.70, x = 1.33	$AB_{2.48}$	77/75/70	4.0	1.60	0.91	–
y = 0.70, x = 1.47	$AB_{2.62}$	65/64/63	–	–	0.97	–

[a]Full hydrogen capacity, corresponds to the highest hydrogen pressure in PCT-curves
[b]Samples do not absorb hydrogen below 50 atm

about 20% increase in the cell volume (Table 2). Superstoichiometric alloys with high manganese content failed to absorb hydrogen below 50 atm. One exception is the $Ti_{0.45}Zr_{0.55}Ni_{0.70}V_{0.45}Mn_{1.33}$ alloy which formed a hydride below 50 atm.

For all hydrogenizing alloys, pressure-composition-temperature (PCT) curves were measured at temperatures in the interval from 0 to 90 °C.

From the data obtained, hydrogen desorption isotherms were plotted. Figure 2 shows the isotherms at 23 °C. The amount of absorbed hydrogen (i.e., hydrogen capacity) and the equilibrium hydrogen pressure are listed in Table 2. The equilibrium hydrogen pressure was estimated as a pressure in the middle of the hydrogen desorption plateau in the isotherm. Samples of the $Ti_{0.45}Zr_{0.55}Ni_{0.85}V_{0.45}Mn_x$ series with $x = 0.10$, 0.18, the $Ti_{0.45}Zr_{0.55}Ni_{0.70}V_{0.45}Mn_x$ series with $x = 0.08$, 0.17, 0.35, 0.53, and the $Ti_{0.45}Zr_{0.55}Ni_{1.0}V_{0.45}Mn_{0.09}$ composition have the plateaus at low pressures (< 0.01 atm.) at the temperatures 20–90 °C, which falls beyond the accuracy limit of our method.

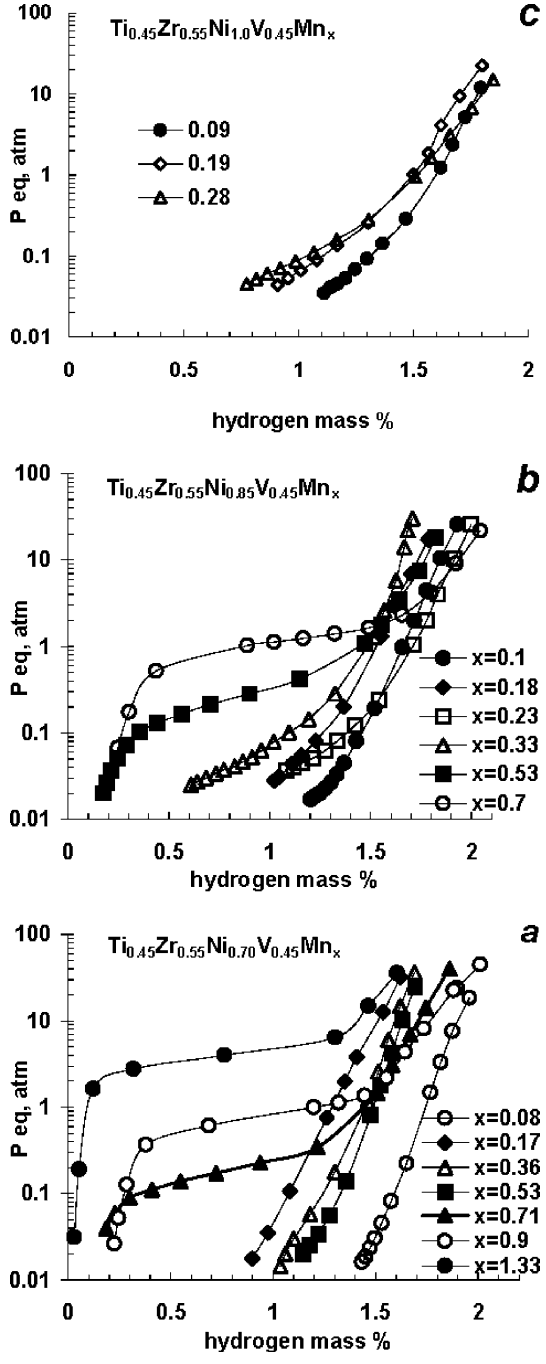

Fig. 2 PCT desorption isotherms of $Ti_{0.45}Zr_{0.55}Ni_yV_{0.45}Mn_x$ alloys at 23 °C

As seen from Fig. 2 and Table 2, the equilibrium hydrogen pressure increases with an increase in the manganese content and depends little on the nickel content. Hydrogen pressures of most IMC hydrides are essentially below 1 atm, making it possible to use these alloys as MH-electrodes.

From equilibrium pressures at different temperatures, the enthalpy and entropy of hydride formation were estimated according to the Vant-Hoff equation and are shown in Table 3. The enthalpy values vary from −4 to −28 kJ/mol. It is known [4] that for a composition to be applicable in Ni-MH batteries its enthalpy should fit between −15 and −50 kJ/mol. The lower values (in absolute terms) correspond to too unstable hydrides formed, whereas, for the higher enthalpies the hydrides formed are too stable and fail to decompose. Most of compositions shown in Table 3 fit the mentioned range. As shown at Table 3, the values of ΔH and ΔS increased with an increase in the manganese content in each series of IMC. Therefore alloys with minimum manganese content are most stable.

Figure 3 shows the dependences of the hydrogen content in the alloys on the manganese content and stoichiometry. Every point in the figure was obtained in several experiments. Hence, despite the rather small number of points in the curves, certain conclusion can be drawn from their complicated shapes, especially, if one compares them with the results of electrochemical measurements shown below. It should also be noted that hydrides of alloys with the minimum hydrogen content, which exhibit significant hydrogen capacities cannot be applied electrochemically due to their relative stability.

The electrochemical behavior of alloys was characterized by the values of their discharge capacities shown

Table 3 Thermodynamic parameters of IMC hydrides

Alloys composition $Ti_{0.45}Zr_{0.55}Ni_yV_{0.45}Mn_x$	n in ABn.	Δ H, kJ/mol	Δ S, J/Mol K
$Ti_{0.45}Zr_{0.55}Ni_{1.0}V_{0.45}Mn_{0.09}$	1.54	−41.7 ± 1.5	−109.1 ± 4.8
$Ti_{0.45}Zr_{0.55}Ni_{1.0}V_{0.45}Mn_{0.19}$	1.64	−39 ± 4	−105 ± 12
$Ti_{0.45}Zr_{0.55}Ni_{1.0}V_{0.45}Mn_{0.28}$	1.73	−36.9 ± 0.2	−104.4 ± 0.6
$Ti_{0.45}Zr_{0.55}Ni_{0.85}V_{0.45}Mn_{0.23}$	1.53	−47.6 ± 8.7	−133.8 ± 28
$Ti_{0.45}Zr_{0.55}Ni_{0.85}V_{0.45}Mn_{0.33}$	1.63	−44.2 ± 2.3	−125.7 ± 7.6
$Ti_{0.45}Zr_{0.55}Ni_{0.85}V_{0.45}Mn_{0.53}$	1.83	−36.4 ± 0.4	−113.3 ± 1.1
$Ti_{0.45}Zr_{0.55}Ni_{0.85}V_{0.45}Mn_{0.70}$	2.00	−32.8 ± 1.1	−112.0 ± 3.6
$Ti_{0.45}Zr_{0.55}Ni_{0.70}V_{0.45}Mn_{0.53}$	1.68	−54.8 ± 6.2	−153 ± 19
$Ti_{0.45}Zr_{0.55}Ni_{0.70}V_{0.45}Mn_{0.71}$	1.86	−35.6 ± 0.4	−108.1 ± 1.2
$Ti_{0.45}Zr_{0.55}Ni_{0.70}V_{0.45}Mn_{0.9}$	2.05	−32.3 ± 0.1	−108.6 ± 0.4
$Ti_{0.45}Zr_{0.55}Ni_{0.70}V_{0.45}Mn_{1.33}$	2.48	−28.3 ± 2.0	−107.9 ± 6.9

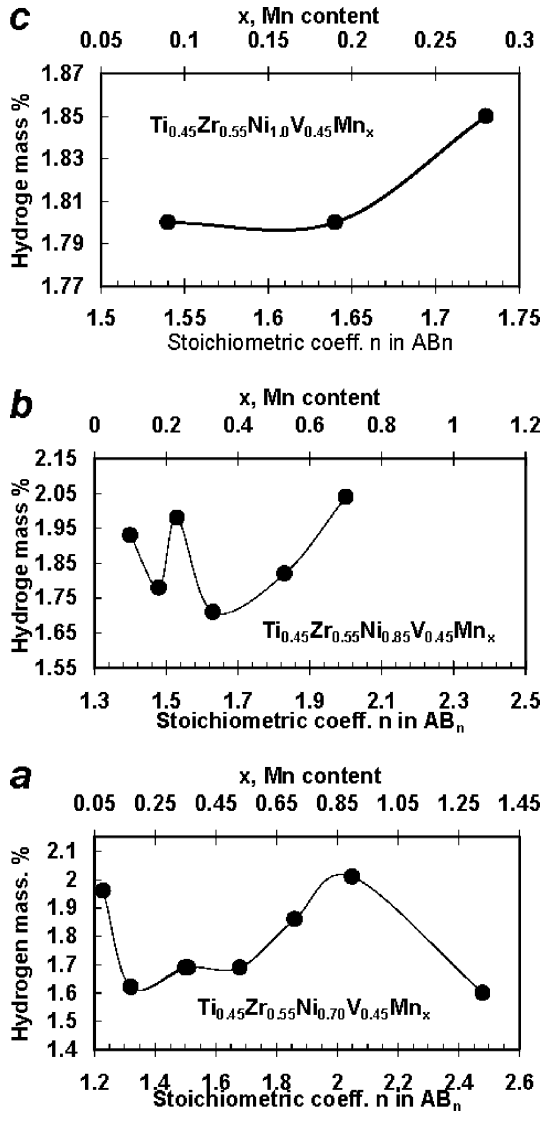

Fig. 3a–c Dependence of hydrogen mass content of: **a** $Ti_{0.45}Zr_{0.55}Ni_{0.85}V_{0.45}Mn_x$; **b** $Ti_{0.45}Zr_{0.55}Ni_{0.70}V_{0.45}Mn_x$; **c** $Ti_{0.45}Zr_{0.55}Ni_{1.0}V_{0.45}Mn_x$ alloys on manganese content and stoichiometry

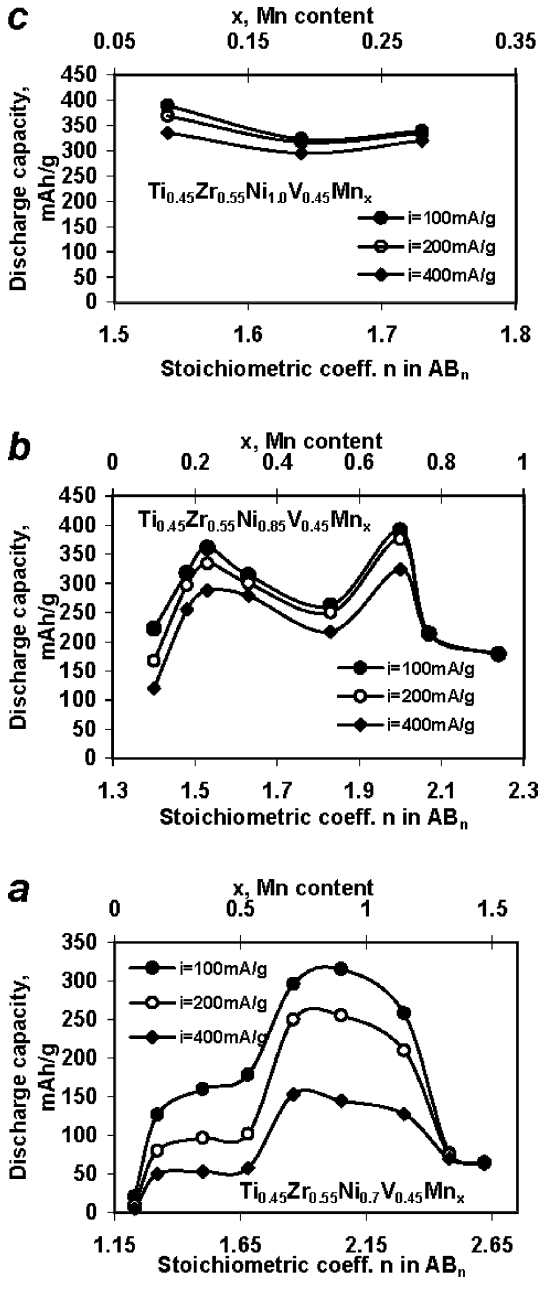

Fig. 4a–c Dependence of discharge capacities of: **a** $Ti_{0.45}Zr_{0.55}Ni_{0.70}V_{0.45}Mn_x$; **b** $Ti_{0.45}Zr_{0.55}Ni_{0.85}V_{0.45}Mn_x$; **c** $Ti_{0.45}Zr_{0.55}Ni_{1.0}V_{0.45}Mn_x$ alloys on manganese content and stoichiometry

in Fig. 4 as a function of the stoichiometry and manganese content. As seen from Fig. 4, the dependence of the discharge capacity on the manganese content has a complicated shape with two maximums for the $Ti_{0.45}Zr_{0.55}Ni_{0.85}V_{0.45}Mn_x$ series and a maximum with a shoulder for the $Ti_{0.45}Zr_{0.55}Ni_{0.70}V_{0.45}Mn_x$ series.

The simple shape of the dependence for the third series, namely $Ti_{0.45}Zr_{0.55}Ni_{1.0}V_{0.45}Mn_x$, is explained by the too narrow range of compositions studied. It should be noted that the shape of these curves much resembles that of similar dependences found in the gas phase (Fig. 3). The discharge curves for best samples are shown at Fig. 5.

To explain the observed dependences, several factors should be considered. First of all, the electrochemical behavior should depend on the stoichiometric factor (n in AB_n) and the presence in the alloy of other phases, which appear with deviation from stoichiometry (Table 1). The maximum of the discharge capacitance corresponds to the stoichiometric composition of the alloys. On the other hand, the lattice cell volume and the size of tetrahedral interstitials, which decrease with the increase in the Mn content, should also affect the hydrogen content in the alloys and, together with the appearance of new phases, can be responsible for the abrupt decrease in the discharge capacitance at high Mn contents. Indeed, the hydrogen content decreases as the lattice cell shrinks. Moreover, the affinity of alloy components to hydrogen (Mn is not a hydride-forming element) should also be taken into account. As to the midconcentration range,

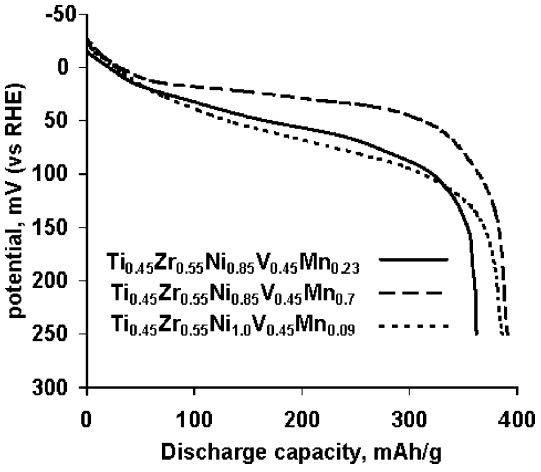

Fig. 5 The discharge curves for $Ti_{0.45}Zr_{0.55}Ni_{0.85}V_{0.45}Mn_{0.23}$, $Ti_{0.45}Zr_{0.55}Ni_{0.85}V_{0.45}Mn_{0.70}$, and $Ti_{0.45}Zr_{0.55}Ni_{1.0}V_{0.45}Mn_{0.09}$ alloys

one more factor acts in this region, namely the changes in the site occupation of the C14 structure, which were revealed in the structural studies. This factor can lead to changes in the type of tetrahedral interstitials and, as a result, to local changes in the hydrogen storage capacity.

The rate capability is yet another factor that should be taken into account when designing a MH battery. As seen from Table 2 and Fig 4, the discharge capacity decreases almost proportionally with an increase in the discharge current density. This follows from the fact that the dependences tend to retain their shape at different current densities. However, the complicated character of their shape makes it impossible to accurately estimate the dependence of the rate capability on the Mn content and allows one only to assess the average rate capability for each alloy. Thus, for the $Ti_{0.45}Zr_{0.55}Ni_{0.85}V_{0.45}Mn_x$ alloy, the average rate capability is about 0.5. For $Ti_{0.45}Zr_{0.55}Ni_{0.70}V_{0.45}Mn_x$ and $Ti_{0.45}Zr_{0.55}Ni_{1.0}V_{0.45}Mn_x$ alloys, the average rate capability is 0.9.

Conclusion

Thus, the alloys studied demonstrate high sorption capacities with respect to hydrogen not only in the vicinity of their stoichiometric compositions (AB_2), but also throughout a wide range of compositions. The most promising compositions are $Ti_{0.45}Zr_{0.55}Ni_{0.85}V_{0.45}Mn_{0.23}$, $Ti_{0.45}Zr_{0.55}Ni_{0.85}V_{0.45}Mn_{0.7}$, and $Ti_{0.45}Zr_{0.55}Ni_{1.0}V_{0.45}Mn_{0.09}$, because they exhibit high values of hydrogen sorption and discharge capacities and the rate capabilities approaching 0.9. However, before making conclusions on the prospects of these alloys, one must test their corrosion behavior, because Mn and V are known to be among the most electrochemically active elements. To improve the corrosion stability, small amounts of Cr may be added to the alloys [13, 17].

References

1. Hamann CH, Hamnett A, Vielstich W (1998) Electrochemistry. Wiley-VCH
2. Vielstich W, Lamm A, Gasteiger H (2003) Handbook of fuel cell technology. Wiley
3. Petrii OA, Vasina SY, Korobov II (1996)Usp Khim 65:195
4. Kleperis J, Wójcik G, Czerwinski A, Skowronski J, Kopczyk M, Beltowska-Brzezinska M (2001) J. Solid State Electrochem 5:229
5. Waterstrat RM, Das BN, Beck PA (1961) Trans Am Inst Min Metall 225:687
6. Schlesinger ME (1999) J Phase Equilib 20(1):79
7. Gamo T, Moriwaki Y, Yanagihara N, Yamashita T, Iwaki T (1980) Third World Hydrogen Energy Conference, vol 4, p 2127
8. Essen van RM, Buschow KHJ (1980) Mater Res Bull 15:1149
9. Okamoto H (1998) J Phase Equilib 19(1):93
10. Yoshida M, Akiba E (1995) J Alloys Compd 224:121
11. Lee H-H, Lee K-Y, Lee J-Y (1997) J Alloys Compd 253/254:601
12. Jung J-H, Lee H-H, Kim D-M, Jang K-J, Lee J-Y (1998) J Alloys Comp 266:266
13. Kim J-S, Paik CH, Cho WI, Cho BW, Yun KS, Kim SJ (1998) J Power Sources 75:1
14. Kim D-M, Jeon S-W, Lee J-Y (1998) J Alloys Compd 279:209
15. Kim D-M, Lee H, Cho K, Lee J-Y (1999) J Alloys Compd 282:261
16. Kim D-M, Jang K-J, Lee J-Y (1999) J Alloys Compd 293/295:583
17. Verbetsky VN, Petrii OA, Vasina SY, Bespalov AP (1999) Int J Hydrogen Energy 24:247
18. Zotov TA, Verbetsky VN, Petrii OA (2002) Hydrogen Mater Sci Chem Metal Hydrides 82:229
19. Petrii OA, Mitrokhin SV, Verbetsky VN, Zotov TA (2002) Proceedings of International Symposium on Metal Hydrogen Systems, p 130